AGU PUBLICATIONS

JGR

Journal of Geophysical Research: Space Physics

RESEARCH ARTICLE
10.1002/2014JA020603

Key Points:
- Bursty enhancements of ≳0.5 keV electrons sometimes occur in the magnetosheath
- Magnetospheric electrons are likely the source
- Enhancement can have a thin and elongated structure

Correspondence to:
C.-P. Wang,
cat@atmos.ucla.edu

Citation:
Wang, C.-P., X. Xing, T. K. M. Nakamura, L. R. Lyons, and V. Angelopoulos (2014), Source and structure of bursty hot electron enhancements in the tail magnetosheath: Simultaneous two-probe observation by ARTEMIS, *J. Geophys. Res. Space Physics*, *119*, doi:10.1002/2014JA020603.

Received 8 SEP 2014
Accepted 21 NOV 2014
Accepted article online 26 NOV 2014

Source and structure of bursty hot electron enhancements in the tail magnetosheath: Simultaneous two-probe observation by ARTEMIS

Chih-Ping Wang[1], Xiaoyan Xing[1], T. K. M. Nakamura[2], Larry R. Lyons[1], and Vassilis Angelopoulos[3]

[1]Department of Atmospheric and Oceanic Sciences, University of California, Los Angeles, California, USA, [2]Space Science and Applications, Los Alamos National Laboratory, Los Alamos, New Mexico, USA, [3]Department of Earth, Planetary, and Space Sciences, University of California, Los Angeles, California, USA

Abstract Bursty enhancements of hot electrons (≳0.5 keV) with duration of minutes sometimes occur in the tail magnetosheath. In this study we used the unique simultaneous measurements from the two Acceleration Reconnection Turbulence and Electrodynamics of Moon's Interaction with the Sun probes to investigate the likely sources, spatial structures, and responsible processes for these hot electron enhancements. The enhancements can be seen at any distance across the magnetosheath, but those closer to the magnetopause are more often accompanied by magnetosheath density and flow magnitudes changing to more magnetosphere-like values. From simultaneous measurements with the two probes being on either side of magnetopause or both in the magnetosheath, it is evident that these hot electrons come from the magnetosphere near the current sheet without further energization and that the enhancements are a result of bursty lateral magnetosphere intrusion into the magnetosheath, the enhancements and changes in the magnetosheath properties becoming smaller with increasing outward distance from the intrusion. From limited events having specific separation distances and alignments between the probes, we estimated that a single isolated enhancement can have a thin and elongated structure as narrow as 2 R_E wide in the X direction, as long as over 7 R_E in the Y direction, and as thin as 1 R_E in the Z direction. We propose that Kelvin–Helmholtz perturbations at the magnetopause and subsequent magnetosphere-magnetosheath particle mixing due to reconnection or diffusion can plausibly play an important role in generating the bursty magnetosphere intrusion into the magnetosheath and the hot electron enhancements.

1. Introduction

The typical thermal energy of the magnetosheath electrons is ~0.04 keV on the dayside and decreases to ~0.015 keV in the tail ($X < -30\ R_E$) [*Wang et al.*, 2012]. Sometimes, strong and bursty enhancements of electron fluxes can be seen in the magnetosheath at energies above ~0.5 keV. Since this is much higher than the magnetosheath thermal energies, in this paper the enhancements are referred to as "hot electron enhancements." The hot electron enhancements can occur in the near-Earth magnetosheath [*Frank et al.*, 1963; *Meng and Anderson*, 1970; *Sarafopoulos et al.*, 1999, 2000; *Imada et al.*, 2005] and in tail magnetosheath [*Sarris et al.*, 1976; *Scholer et al.*, 1984]. It has been suggested that these hot electrons come from either solar wind particles being accelerated at the bow shock, magnetosheath electrons being energized at the magnetopause, or hot electrons from the magnetosphere [*Sibeck and McEntire*, 1988]. *Kudela et al.* [1994] examined the energetic electron fluxes in the solar wind, magnetosheath, and magnetosphere on the dayside and suggested that the enhancements closer to the bow shock are likely due to bow shock acceleration, while those near the magnetopause are from the magnetosphere. *Sarris et al.* [1978] studied bursts of energetic electrons using simultaneous measurements from two satellites: one in the magnetosphere and one in magnetosheath. Their results showed that magnetosphere energetic electron fluxes increased before hot electron enhancements were observed in the magnetosheath, suggesting that the hot electrons in the enhancements originate from the magnetosphere.

Considering the hot magnetosphere electrons as the source for the hot electron enhancements, it has been proposed that they can have access to the magnetosheath either through leakage due to their large gyroradius [*Sibeck et al.*, 1987] or through interconnected magnetosphere-magnetosheath magnetic field

©2014. American Geophysical Union. All Rights Reserved.

lines [*Scholer et al.*, 1981]. Typical thermal energy for the magnetosphere electrons can be up to 10 keV in the inner magnetosphere but is only a few hundreds of eV in the tail [*Wang et al.*, 2012]. The above past observations and proposed responsible processes for the hot electron enhancements focused mainly on energetic electrons from ~15 keV to hundreds of keV in the near-Earth magnetosheath. However, many aspects of the hot electron enhancements in the tail magnetosheath, including their typical energy range, sources, and the responsible processes, remain to be determined. Since late 2010, the two probes from the Acceleration Reconnection Turbulence and Electrodynamics of Moon's Interaction with the Sun (ARTEMIS) mission have been surveying the tail magnetosphere and magnetosheath at the lunar distances (~60 R_E) with varying separations and alignments. The unique simultaneous two-probe measurements allow for better determination of the spatial structures of the hot electron enhancements, thus providing more unambiguous indications of plausible source locations and responsible processes.

In this paper, we investigate the hot electron enhancements in the tail magnetosheath observed by the two ARTEMIS probes. We focus on simultaneous measurements with specific alignments between the two probes that can better reveal the connection between the magnetosheath and magnetosphere and the spatial structures of the enhancements. The ARTEMIS measurements are described in section 2. In section 3, we present the characteristics of the hot electron enhancements and the associated changes in plasma moments and magnetic fields, their connection with the magnetosphere electrons, and determination of their 3-D spatial structures. From these observations, we discuss in section 4 the Kelvin–Helmholtz instability as a plausible process resulting in the hot electron enhancements.

2. Data

We use the particle and magnetic field measurements from the two ARTEMIS probes (AR-B and AR-C) [*Sibeck et al.*, 2011]. The ARTEMIS probes were originally part of the five spacecraft for Time History of Events and Macroscale Interactions during Substorms (THEMIS) mission in the near-Earth magnetosphere. They started to move outward in early 2010 to their final orbits at the lunar distances (r~60 R_E). It takes roughly 2 days for each probe to laterally cross the duskside or dawnside magnetosheath, while the separation distances and alignment directions between the two probes keep changing as they move. The two probes were first separated with large distances in 2010 and early 2011 but later approached each other. In this study, we investigate the observations from August 2011 to December 2013. The maximum separation during the month of August 2011 is ~8 R_E. From September 2011 to December 2013, the maximum separation varies from ~3 to 5.7 R_E, while the minimum separation varies from as small as $<$0.1 R_E to ~2 R_E. The Z separation in geocentric solar ecliptic (GSE) coordinates is always smaller than ~0.9 R_E. Thus, the two probes become well separated in the X-Y plane when the separations are larger. The alignments in the X-Y plane can be along any direction.

For ions and electrons, we use measurements by an electrostatic analyzer (ESA; 0.006–20 keV/q [*McFadden et al.*, 2008]). The magnetic field is measured by the fluxgate magnetometer [*Auster et al.*, 2008]. Onboard plasma moments, omnidirectional energy fluxes, and magnetic field with ~4 s resolutions are used. Three-dimensional phase space density distributions with ~4 s resolutions are only available for limited times when the instrument is on fast survey mode. Geocentric solar ecliptic (GSE) coordinates are used for the probe locations, but the three components of bulk flow and magnetic field in geocentric solar magnetospheric (GSM) coordinates are used. One-minute solar wind and interplanetary magnetic field (IMF) parameters that have been shifted to the Earth's bow shock nose were used. Additional time shift from the bow shock nose to the ARTEMIS locations estimated using the solar wind speed was then added.

3. Results

3.1. Hot Electron Enhancements in the Magnetosheath

Figures 1 and 2 give overviews of the particles and magnetic fields of the tail magnetosheath observed by the two ARTEMIS probes from two dawnside magnetosheath crossings on 14–15 September 2011 (event 1) and 6–7 June 2012 (event 2), respectively. There were more hot electron enhancements observed during these two crossings than during others. The maximum X-Y separation is ~4 R_E during event 1 but only ~1.5 R_E for event 2. The solar wind speed in event 1 (~450–550 km/s) is slightly higher than the typical value of ~450 km/s, but it is substantially higher in event 2 (~600–700 km/s). The solar wind density is ~1–2 cm^{-3}

©2014. American Geophysical Union. All Rights Reserved.

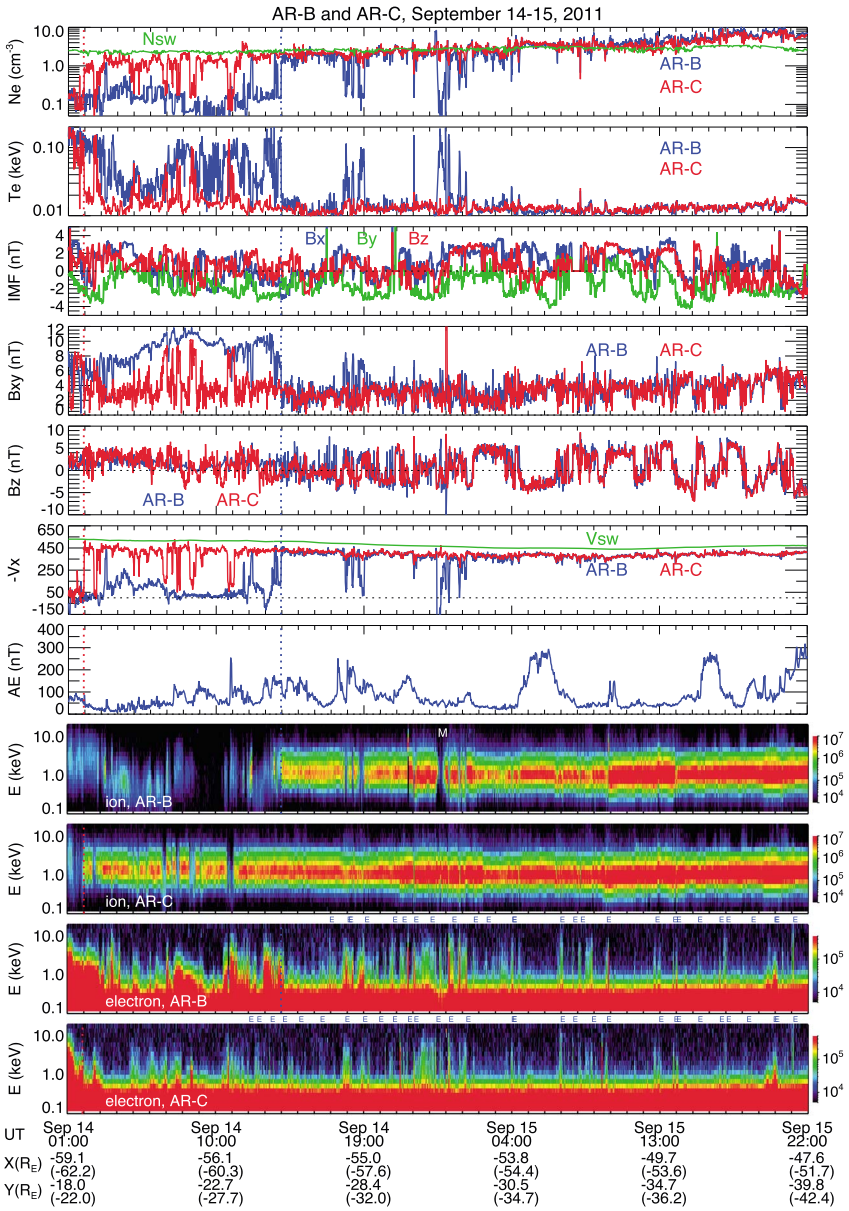

Figure 1. (top to bottom) Electron density, electron temperature, IMF, B_{xy}, B_z, $-V_x$ (the blue curves for AR-B and the red curves for AR-C except in the IMF plot; solar wind density and speed are plotted in green), AE, and omnidirection ion and electron fluxes observed by AR-B and AR-C on 14–15 September 2011. The *X* and *Y* locations are in the GSE coordinates with the locations of AR-C shown inside the parentheses. The white "M" in ion energy flux plot indicates lunar wake crossing. Each blue E on top of the electron energy flux plots marks the peak of hourly maximum hot electron enhancement. All the ion and electron energy fluxes shown in this paper are in eV/(s sr cm^2 eV).

during both events, and the solar wind dynamic pressure is about 1–2 (1–3) nPa in event 1 (2). Compared with the magnetosphere plasma, the magnetosheath plasma is colder (electron temperature is ~0.015 keV) and denser ($>$ ~1 cm^{-3}) with strong tailward flow ($>$ ~300 km/s). The directions of magnetosheath magnetic field resemble the interplanetary magnetic field (IMF). In the magnetosphere, density is substantially lower than 1 cm^{-3}, electron temperature is above ~0.1 keV, and bulk flow speed is smaller than ~200 km/s most of the time. There are three main plasma regions inside the magnetosphere: the plasma sheet, the lobes, and the mantles. Plasma is hotter and slower in the plasma sheet but the colder and denser tailward flowing mantle plasma with magnetosheath-like properties, but reduced density and flow speed, can sometimes appear in the lobes, like the plasma observed by AR-B from ~3 to 7 UT on 14 September 2011 shown in

©2014. American Geophysical Union. All Rights Reserved.

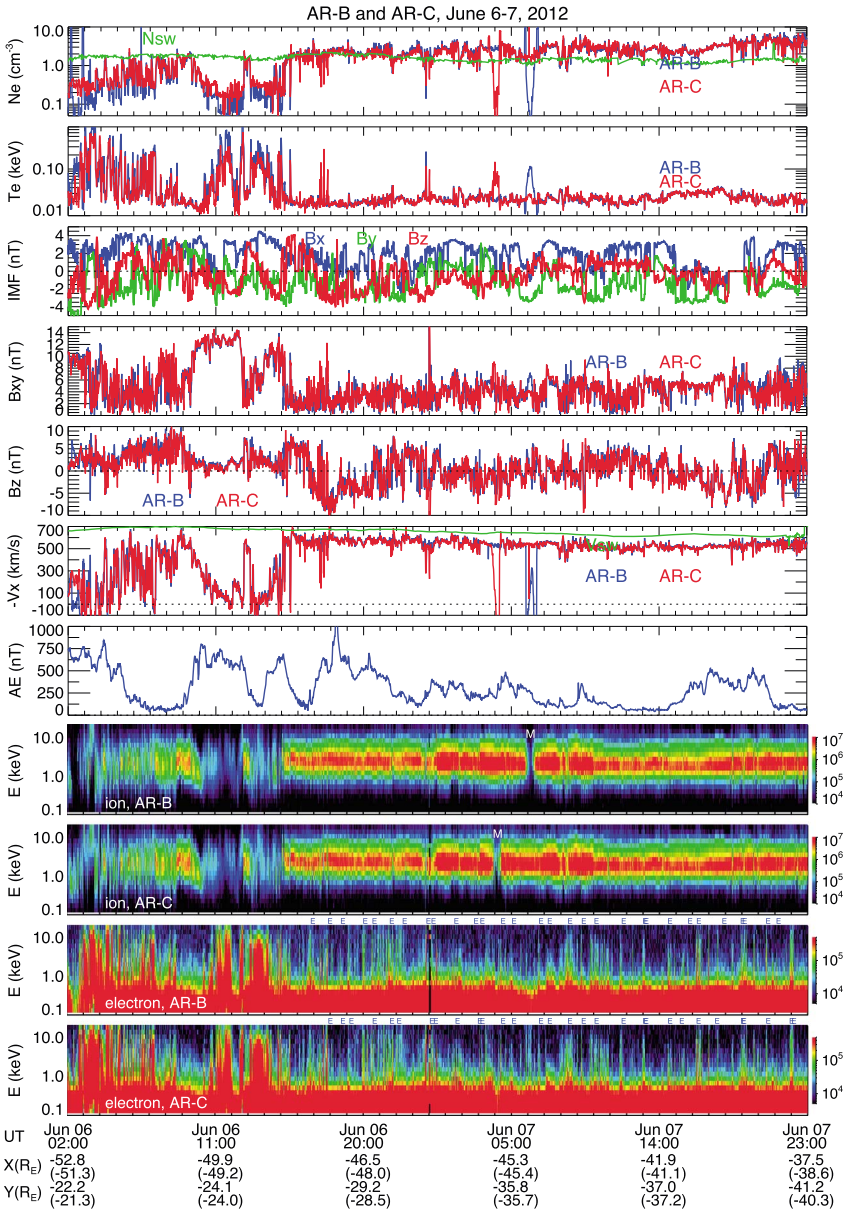

Figure 2. (top to bottom) Electron density, electron temperature, IMF, B_{xy}, B_z, $-V_x$ (the blue curves for AR-B and the red curves for AR-C except in the IMF plot; solar wind density and speed are plotted in green), AE, and omnidirection ion and electron fluxes observed by AR-B and AR-C on 6–7 June 2012. The *X* and *Y* locations are in the GSE coordinates with the locations of AR-C shown inside the parentheses. The white M in ion energy flux plot indicates lunar wake crossing. Each blue E on top of the electron energy flux plots marks the peak of hourly maximum hot electron enhancement.

Figure 1. B_z in the magnetosphere is mostly positive and B_{xy} is larger with increasing *Z* distance from the current sheet center (the center is defined in this paper as $B_{xy} = 0$, and *Z* is the direction perpendicular to the current sheet plane). In event 1, AR-C crossed the magnetopause at $Y\sim -23\ R_E$ at 01:56 UT, and AR-B crossed it later at $Y\sim -25\ R_E$ at 13:57 UT on 14 September 2011 (indicated by the vertical dotted lines). While in event 2, multiple magnetopause crossings were encountered by the two probes from ~4 to 7 UT on 6 June 2012 at $Y\sim -22\ R_E$. The probes were then back again into the magnetosphere likely due to the magnetopause moving outward and stayed inside the magnetosphere until the last magnetopause crossing at ~15 UT on 6 June 2012 at $Y\sim -26\ R_E$. The bow shock crossings are at $Y\sim -49$ (-43) R_E for event 1 (2) (the time of the bow shock crossings were later than the periods shown in Figures 1 and 2). Thus, the magnetosheath width at $X\sim -40$ to $-60\ R_E$ is about 20 R_E.

©2014. American Geophysical Union. All Rights Reserved.

In the magnetosheath, the ion omnidirectional energy fluxes are seen to peak at $>$ ~1 keV. However, the ion thermal energy is ~0.1 keV, and the $>$1 keV peak is due to a shift in the phase space density by the large magnetosheath bulk velocity. On the other hand, the shift is much smaller for electrons (for example, 400 km/s corresponds to electron energy of ~0.4 eV, while magnetosheath electron thermal energy is ~15 eV). Thus, any changes in electron fluxes seen above the thermal energy are not due to changes in magnetosheath flow speed. As the probes laterally crossed the magnetosheath, they often observed large and busty increases in electron energy fluxes at energies above ~0.5 keV. These increases are referred to as hot electron enhancements since these electrons are quite hot relative to the magnetosheath thermal population. In this study, we consider an increase as a hot electron enhancement if the peak value of the 1 keV electron energy flux is at least a factor of 5 higher than the median value of the 1 keV magnetosheath electrons computed from the data within that magnetosheath crossing. The peaks of the hourly maximum enhancements are indicated by the blue "E" on top of the electron energy flux plots in Figures 1 and 2. It can be seen that these enhancements are not due to an increase in electron density. In event 1, the hot electron enhancements appear more frequently closer to the magnetopause, while in event 2, their occurrence remained frequent across the magnetosheath.

The duration of a hot electron enhancement can vary from ~1 to $>$10 min as can be seen in the four examples shown in Figure 3. Some enhancements have only one single strong peak with a short duration of ~1 to a few minutes, like those shown in Figures 3a and 3b. Other enhancements have several individual peaks being very close to each other, so that the enhancement appears more continuous and lasts longer, like the one shown in Figure 3c and the first enhancement in Figure 3d. During a hot electron enhancement, the magnetosheath plasma moments and magnetic fields sometimes also undergo changes, and the changes can be quite different for each enhancement. The single enhancement shown in Figure 3a is associated with large decreases in density and flow speed but increases in temperatures, with these values becoming closer to those of magnetosphere plasma. The single enhancement shown in Figure 3b is also associated with density and temperature changes, but the changes are much smaller than those in Figure 3a. Another difference is that there is almost no change in flow speed associated with the enhancement in Figure 3b. On the other hand, the enhancements shown in Figures 3c and 3d do not have any substantial change in any of the plasma moments. In terms of magnetic fields, they changed significantly during the enhancements shown in Figures 3a, 3b, and 3d, but there is almost no change associated with the enhancement shown in Figure 3c. As can be seen in Figures 1 and 2, enhancements closer to the magnetopause are more often accompanied by larger decreases in density and flow speed. The comparisons shown in Figure 3 (bottom) between energy spectra with (red curves) and without (blue curves) a hot electron enhancement show that the enhancements result from hot electrons of ~0.5 to 5 keV being added to the cold magnetosheath population. The enhancements sometimes extend up to $>$10 keV. No energy dispersion is seen for the enhancements. For example, Figure 3d shows that the fluxes for 1 and 10 keV electrons reached their peaks at the same time. In the following sections, we use the hot electron enhancements simultaneously observed by AR-B and AR-C during the two events and from other crossings to show that the hot electrons in the enhancements shown in Figure 3 with different changes in the magnetosheath properties are likely all from the magnetosphere and are a result of the same process.

3.2. Connection of Hot Electron Enhancements With the Magnetosphere

Figures 4a and 4b show simultaneous observations with AR-B being in the magnetosphere, while AR-C, being ~4 R_E away from AR-B, was in the magnetosheath and observed the hot electron enhancements. There are large decreases in density and flow speed associated with the enhancements, like the one shown in Figure 3a. It can be seen that the density, flow speed, the magnetic field components, and the 1 keV energy fluxes at the time of the enhancements all changed to values similar to those of the magnetosphere observed by AR-B. This simultaneous observation strongly indicates that the hot electrons in these enhancements seen by AR-C are magnetosphere electrons. The very abrupt and brief encounter of the magnetosphere-like plasma and magnetic fields by AR-C is likely a result of magnetosphere plasma and magnetosphere fields intruding locally into the magnetosheath (we refer this to as magnetosphere intrusion) rather than due to outward motion of the dawnside magnetopause, since there was no sharp and substantial change in either solar wind dynamic pressure or IMF around the times of these enhancements. To illustrate our suggested locations of the two probes with respect to the magnetosphere, magnetosheath, magnetopause, magnetosphere intrusion, and the

©2014. American Geophysical Union. All Rights Reserved.

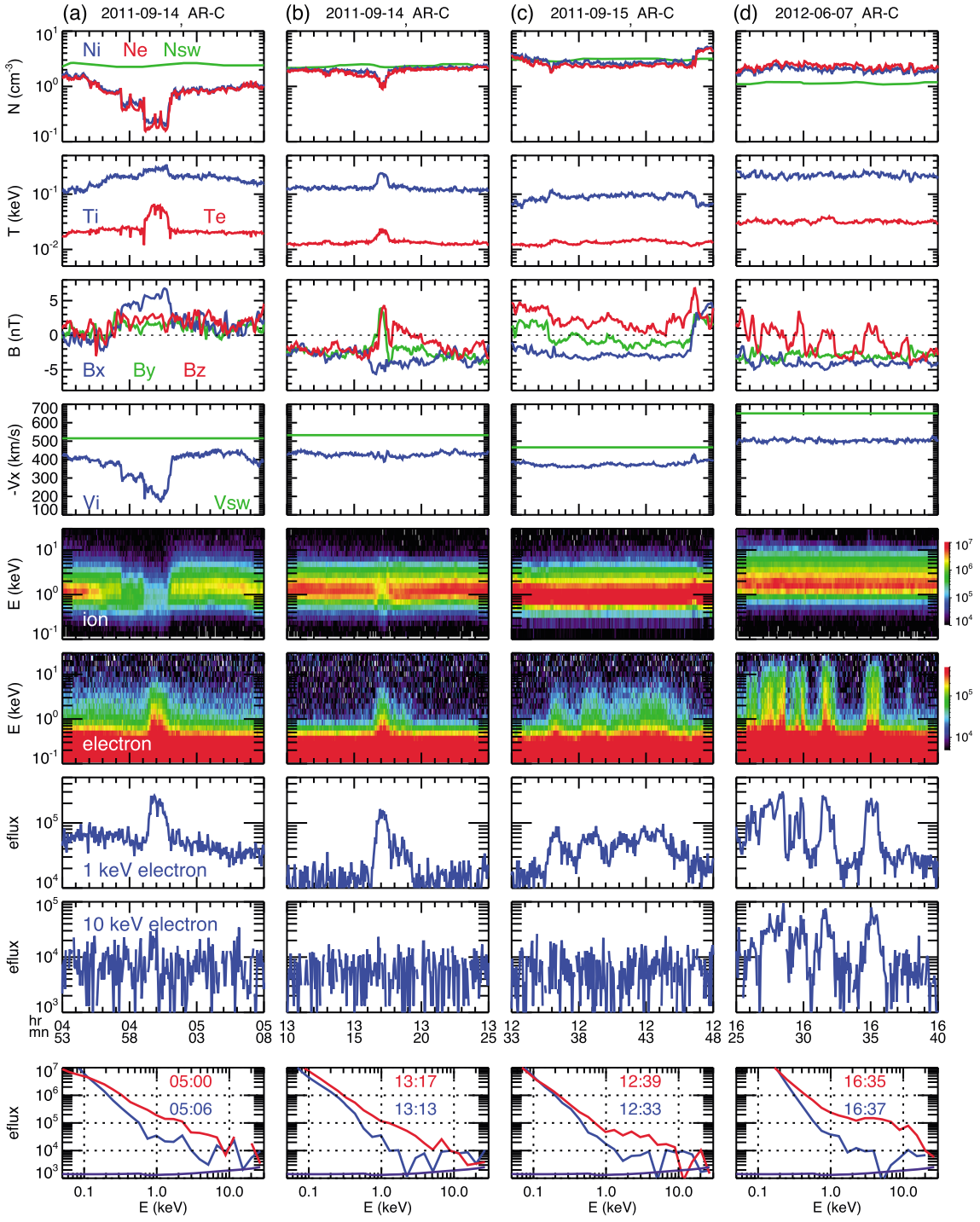

Figure 3. Hot electron enhancements observed by AR-C. (top to bottom) Densities, temperatures, magnetic fields, flow speeds, ion and electron energy fluxes, 1 and 10 keV electron energy fluxes, and electron energy fluxes versus energy (the purple curves indicate fluxes correspond to 1 count).

hot enhancements, we plot their locations in the *X-Y* and *Y-Z* planes in Figures 5a and 5b, respectively. Note that the region of the hot electron enhancement includes those inside and outside the magnetosphere intrusion, with plasma and field inside (outside) the magnetosphere intrusion being more magnetosphere-like (magnetosheath-like), and the arrow with white dashed lines indicates the processes moving magnetosphere hot electrons to outside the intrusion. The likely processes creating this bursty magnetosphere intrusion and hot electron enhancements will be discussed in section 4. For comparison, in the example shown in Figure 4c,

©2014. American Geophysical Union. All Rights Reserved.

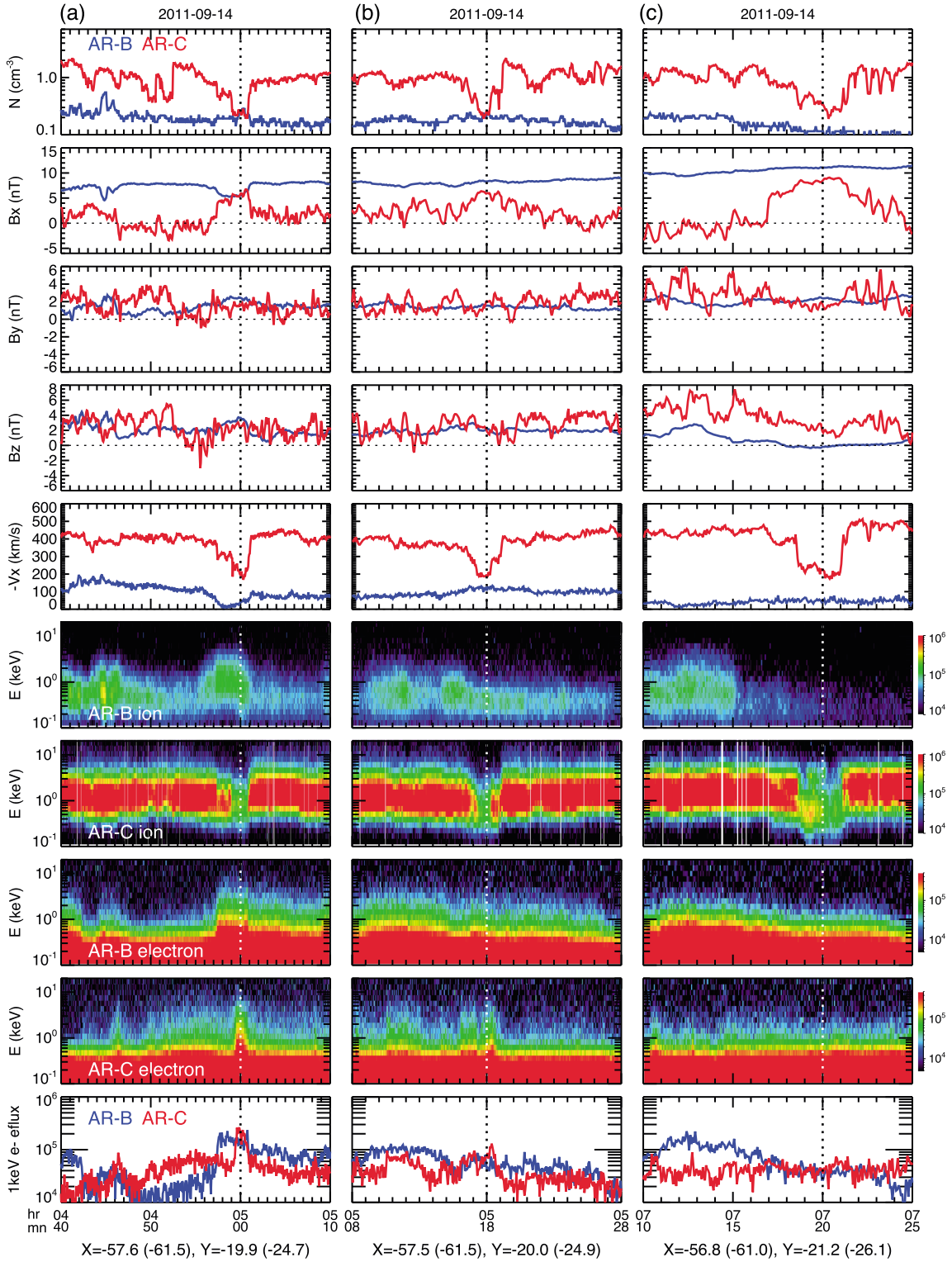

Figure 4. (top to bottom) Ion densities, magnetic fields, flow speeds, ion and electron energy fluxes, and 1 keV electron energy fluxes observed by AR-B in the magnetosphere (the blue curves) and by AR-C in the magnetosheath (the red curves). The *X* and *Y* locations for AR-C are indicated inside the parentheses.

©2014. American Geophysical Union. All Rights Reserved.

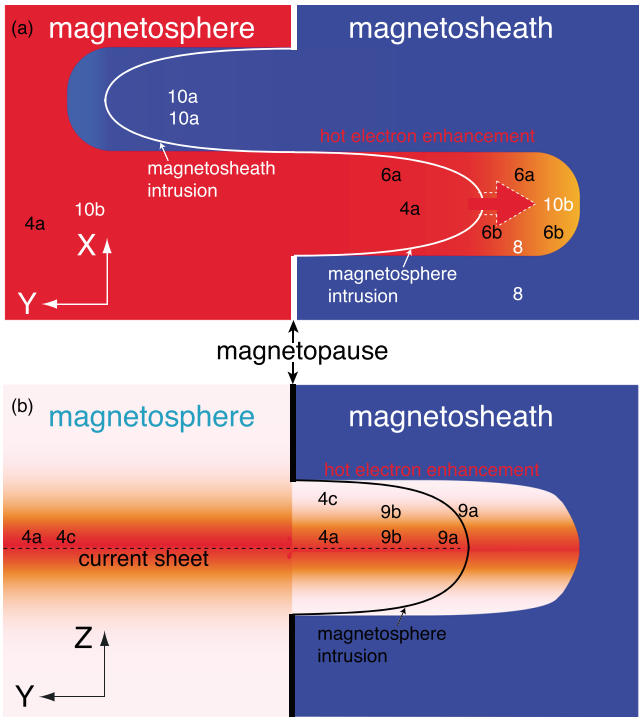

Figure 5. Schematic illustration of the locations of the two probes in (a) *X-Y* and (b) *Y-Z* planes when they simultaneously observed the enhancements shown in Figures 4a, 5a, 5b, 7b, 8, and 9b (each figure number is indicated at the two probe locations). The bluish color represents the cold magnetosheath electron fluxes, and the reddish color represents the hot magnetosphere electron fluxes, with brighter color indicating lower fluxes. The white solid lines in Figure 5a and the black solid curves in Figure 5b indicate the boundary separating the magnetosphere and the magnetosheath magnetic field. The arrow indicated by the white dotted line in Figure 5a represents the electrons crossing the magnetic field boundary. The black dotted line in Figure 5b indicates the center of the current sheet.

density, flow speed, and magnetic fields observed by AR-C all changed to magnetosphere values, like those shown in Figures 4a and 4b, suggesting that AR-C encountered magnetosphere intrusion. However, AR-C observed no hot electron enhancement associated with the intrusion. As discussed later, hot electron fluxes in the magnetosphere decrease quickly with increasing Z distances (or increasing B_{xy}) from the current sheet center to values as low as those of the magnetosheath electrons. Thus, as illustrated in Figure 5, AR-C may encounter a portion of intruding magnetosphere that is too far away from the current sheet center to have significant magnetosphere electron fluxes to cause any flux increase. The spatial structures of the hot electron enhancements in the X, Y, and Z directions are investigated in section 3.3.

Figure 6 shows examples of hot electron enhancements that occurred simultaneously at the AR-B and AR-C locations, while the two probes were both in the magnetosheath and were at almost the same X ($<1\ R_E$) but with a large Y separation ($\gtrsim 4\ R_E$). The same X condition is for the simultaneity because that, as will be shown in the next section, there is a time lag for most of the enhancements observed by the two probes when they were well separated in X. The two strong enhancements observed by AR-B shown in Figure 6a are accompanied by large changes in plasma moments and magnetic fields as if the probe encountered magnetosphere intrusion, similar to the enhancements shown in Figure 3a and Figures 4a and 4c. At the same time, AR-C was 4 R_E further outward in Y and observed enhancements but with much smaller increases in hot electron fluxes and smaller changes in the magnetosheath plasma moments and magnetic fields, like the one shown in Figure 3b. The simultaneity of the observations clearly indicates that the hot electron enhancements seen by AR-C are directly connected with the same magnetosphere intrusions seen by AR-B, and thus, the hot electrons in the enhancements at the AR-C location should also be those coming out from the magnetosphere. Since there were only small changes in the magnetosheath properties seen by AR-C (so more magnetosheath-like), it is likely that AR-C was located outside of the intrusion, as illustrated in Figure 5.

In the example shown in Figure 6b, the density and flow speed observed by AR-B decreased associated with the enhancement, but the changes are relatively small, like the one observed by AR-C in Figure 6a. At the same time, AR-C, being 4 R_E further outward, also observed hot electron enhancements but with an even smaller decrease in density than that at AR-B and with no change in flow speed. From the small changes in the magnetosheath properties, both AR-B and AR-C should be outside the magnetosphere intrusion, as illustrated in Figure 5. Similarly, Figure 6c shows hot electron enhancements occurring simultaneously at the AR-B and AR-C locations 4 R_E apart, with both being associated with almost no changes in density and flow speed. Another similar example is shown in Figure 6d but with an even larger Y separation of 7 R_E. Note that this is the largest Y separation we found in ARTEMIS data for an enhancement observed simultaneously

©2014. American Geophysical Union. All Rights Reserved.

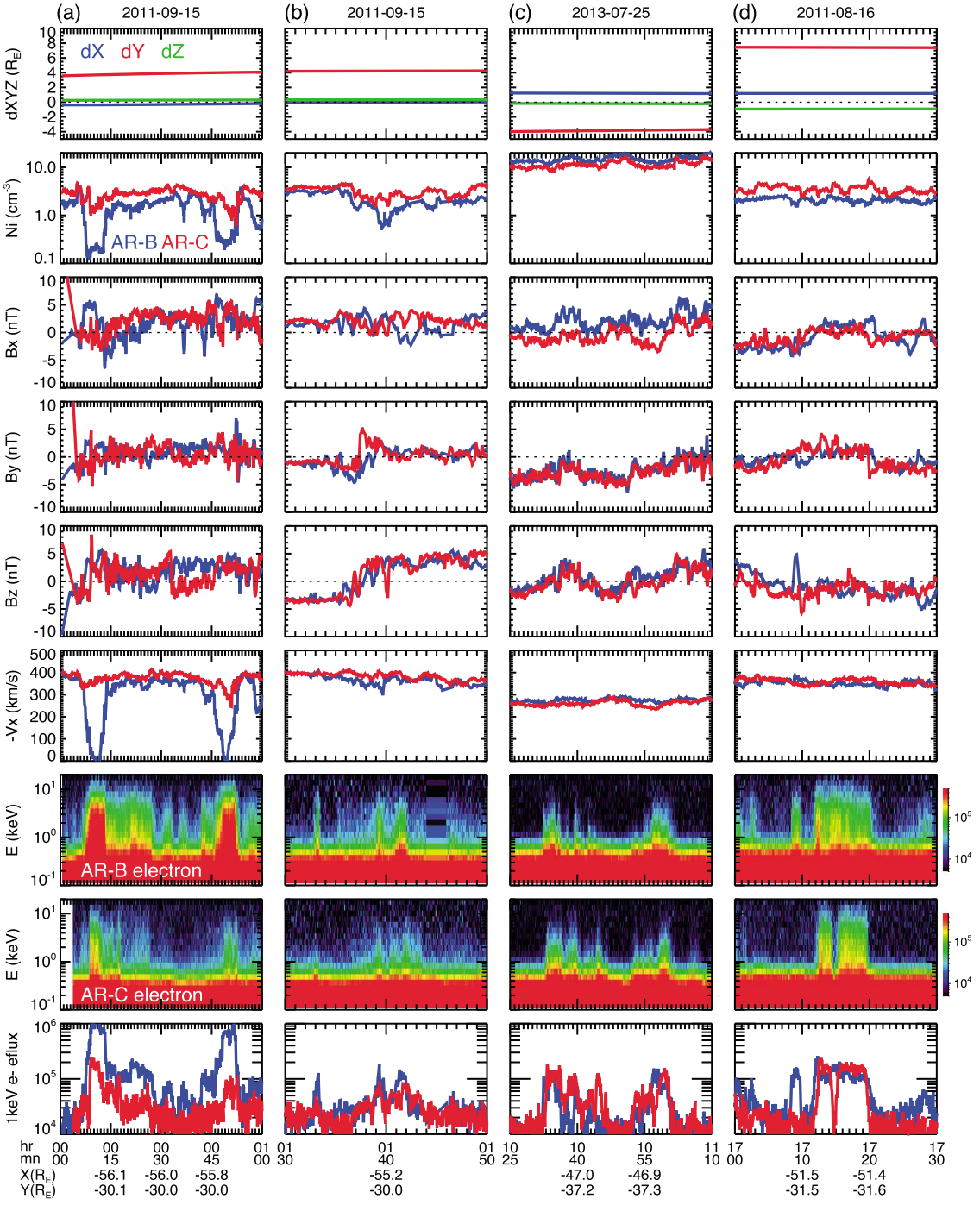

Figure 6. Simultaneous measurements of hot electron enhancements from AR-B and AR-C. (top) Location differences in *X* (blue), *Y* (red), and *Z* (green) (e.g., $dX = X_{AR\text{-}B} - X_{AR\text{-}C}$, AR-B locations are shown in the bottom). (second to bottom) Ion densities, magnetic fields, flow speeds, electron energy flux spectrums, and 1 keV electron energy fluxes observed by AR-B (blue curves) and AR-C (red curves).

by the two probes at the same *X*. Before August 2011, the *Y* separations of the two probes were larger than 7 R_E, but their *X* separations were also large.

The direct connection between the two enhancements occurring more than 4 R_E apart shown in Figure 6 indicates that the enhancements with large or small changes in the associated magnetosheath plasma moments and magnetic fields, as represented by the examples shown in Figure 3, can occur simultaneously at different *Y* locations along the same *X* resulting from bursty intrusion of the magnetosphere into the

©2014. American Geophysical Union. All Rights Reserved.

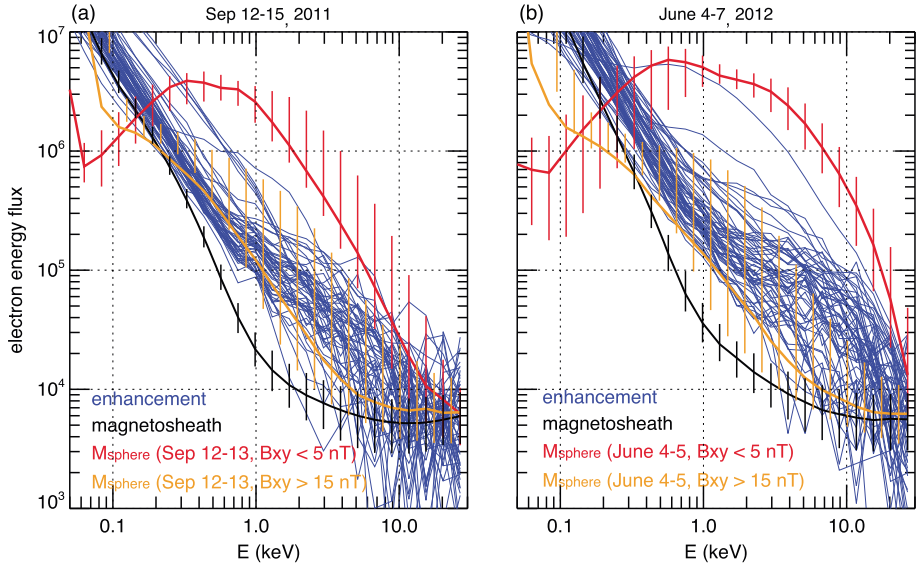

Figure 7. The electron energy spectrums for the peaks of hourly maximum enhancements (the blue curves) for (a) event 1 and (b) event 2. The peaks are marked in Figures 1 and 2 with blue E. Overplotted are the median fluxes for magnetosphere electrons at $B_{xy} < 5$ nT (red curves) and $B_{xy} > 15$ nT (the orange curves), and median fluxes for magnetosheath electrons (black curves) with vertical lines indicate the 25% and 75% quartiles.

magnetosheath along the *Y* direction. It is likely that the magnetosphere intrusion and subsequent processes weaken further outward, causing the smaller increases in hot electron flux and smaller changes in the magnetosheath properties observed by the probe located further away from the magnetopause.

Figure 7 shows more evidence that the hot electrons ($\gtrsim$0.5 keV) in the hot electron enhancements come from the magnetosphere. The electron energy spectra for each of the hourly maximum enhancements indicated by the blue E in Figures 1 and 2, together with the medians of magnetosheath electron fluxes obtained separately from these two crossings, are plotted in Figures 7a and 7b, respectively. For comparison, the median fluxes for the magnetosphere electrons in the dawnside magnetosphere within two different B_{xy} ranges are also plotted in Figure 7. The median magnetosphere fluxes shown in Figures 7a and 7b are computed, respectively, from the magnetosphere electron data within the 2 day periods preceding events 1 and 2 (12–13 September 2011 for event 1 and 4–5 June 2012 for event 2) selected with the criteria: $N_e < 0.5\ \mathrm{cm}^{-3}$, $|V_x| < 50$ km/s, and $0 > Y > -20\ R_E$. From the flux differences between the two B_{xy} ranges, it can be seen that the number of magnetosphere electrons decreases very quickly with increasing *Z* from near the current sheet center ($B_{xy} < 5$ nT, the red curves) to near the lobes ($15 < B_{xy} < 20$ nT, the orange curves). The overall magnetosphere electron energy fluxes are higher during the 4–5 June 2012 period than those during the 12–13 September 2011 period, likely because their corresponding solar wind speed was higher.

It can be seen that the energy fluxes of the maximum hot electron enhancements are well within the flux ranges of magnetosphere electrons and that the enhancements are generally stronger for event 2 during which solar wind speed was higher, consistent with the magnetospheric electron fluxes being higher under higher solar wind speed. Furthermore, despite that overall fluxes decrease with increasing *Z* (or B_{xy}) with their values (the orange curves) becoming closer to those of the magnetosheath electrons (black curves), the fluxes in the range of ~0.5 to 5 keV are still substantially higher than the magnetosheath fluxes compared with other energies. Thus, if these magnetosphere electrons enter the magnetosheath without any energy changes, then they should result in flux enhancements mainly in the 0.5 to 5 keV range, consistent with the typical energies seen for the hot electron enhancements. The above quantitative comparison provides strong indications that the hot electrons in the enhancements are from the magnetosphere without further energization. From the *Z* dependence of magnetosphere electron fluxes, the flux enhancement will be smaller if the hot electrons in the enhancement are from the magnetosphere at larger *Z*. Thus, it is possible that the magnetosphere electron at large *Z* has simply too low fluxes to cause an enhancement when they enter the magnetosheath, like the example shown in Figure 4c.

©2014. American Geophysical Union. All Rights Reserved.

3.3. Spatial Structures of Hot Electron Enhancements

The three examples shown in Figures 6b to 6d with the same enhancements simultaneously observed by the two probes at the same *X* but with large *Y* separations indicate that the *Y* scale of the enhancements can be as large as more than 7 R_E. However, it is likely that the *Y* scale can be even larger considering the distances from the magnetopause to the locations of these observations. For example, during the enhancements shown in Figure 4c, AR-B (AR-C) was at $Y\sim -30$ (-34) R_E, while the last magnetopause crossing was seen by AR-B at $Y\sim -25$ R_E (see Figure 1), suggesting that the enhancements can possibly extend more than 9 R_E from the magnetopause along the *Y* direction.

When the two probes were well separated in *X*, most of the time the hot electron enhancements were observed earlier by the probe closer to the Earth, indicating that the hot electrons are propagating tailward. Figure 8 shows three examples with the two probes being at roughly the same *Y* but with ~4 R_E separations in *X*. The alignment for the two probes with respect to the enhancements is illustrated in Figure 5. The magnetosheath flow speed is low (~300 km/s), median, (~400 km/s), and high (~600 km/s) for these three examples, respectively. It can be seen that the temporal variations of the fluxes observed by the two probes are very similar, with the flux enhancements appearing earlier at locations closer to the Earth. There are also clear time lags in either density, magnetic fields, or flow, as can be identified by tracking sharp changes in these parameters (for example, in the 15 September 2011 example, *N* and B_y observed by AR-B changed sharply at 13:45 UT, which was observed later by AR-C). We shifted the profiles of all parameters observed by AR-B either forward or backward in time with a time difference (*dt*) and plotted the shifted profiles in green to compare with the profiles of AR-C. The values of *dt* are indicated on the "$-V_x$" plots. We then computed the tailward propagation speed ($|dX|/dt$). The estimated propagation speeds, as indicated also on the $-V_x$ plots, are found to be roughly the same as the magnetosheath flow speeds (the probe itself was moving at speed of <1 km/s at the time), which are substantially different for these three cases shown. The good consistency between the time-shifted AR-B profiles and those of AR-C as well as between the propagation speeds and flow speeds confirm that the hot electrons are propagating tailward together with the cold magnetosheath particles and magnetic fields. From the propagation speeds, we estimated that the two single-peaked and isolated enhancements observed by AR-B for the two examples shown in Figures 8b and 8c (indicated by the blue vertical doted lines in the bottom 1 keV flux line plots), respectively, have similar widths of ~2–3 R_E in the *X* direction, which is shorter than the estimated length in the *Y* direction. Thus, each single-peaked hot electron enhancement is likely to have a structure in the *X-Y* plane that is elongated in the *Y* direction.

Sometimes, the two probes can observe quite different variations in plasma moments and magnetic fields associated with the same enhancement even when they were very close to each other. Figures 9a and 9b show three strong hot electron enhancements observed by AR-C (indicated by the vertical dotted lines), each lasted for about 1 min and is only separated from each other by a few minutes. The significant changes in density, flow speed, and magnetic field indicate that AR-C went briefly but deeply within a magnetosphere intrusion when observed the strong hot electron enhancements. On the other hand, AR-B, despite being only about 1.2 R_E away, it observed much weaker flux enhancements, and the densities and flow speeds decreased only slightly in the two enhancements shown in Figure 9a. The magnetic fields observed by AR-B during these two enhancements were changing toward the directions of the magnetosphere-like magnetic fields observed by AR-C, but the changes are much smaller. This suggests that AR-B was near the periphery of the magnetosphere intrusion seen by AR-C, as illustrated in Figure 5. For the enhancement shown in Figure 9b, within the intrusion encountered by AR-C, both B_x and B_y change signs at the time the enhancement reached its peak, indicating that AR-C crossed the current sheet center where electron fluxes are the highest. In comparison, such current sheet center crossing was not observed by AR-B, suggesting that AR-B may only crossed the intrusion that is some *Z* distances away from the current sheet center, as illustrated in Figure 5. Considering the two probes being so close to each other during these three enhancements that occurred only a few minutes apart, the above large differences between the probes suggest that these hot electron enhancements are thin in the *Z* direction, so that plasma moments and magnetic fields vary quickly within the 1 R_E distance from AR-B to AR-C.

Based on the above simultaneous observations of the hot electron enhancements with different separation distances and alignments, a single-peaked hot electron enhancement likely has an elongated and thin spatial structure extending laterally outward from the magnetopause near the magnetosphere current sheet with a width in the *X* direction as narrow as 2 R_E, a length in the *Y* direction as long as more than 7 R_E, and

©2014. American Geophysical Union. All Rights Reserved.

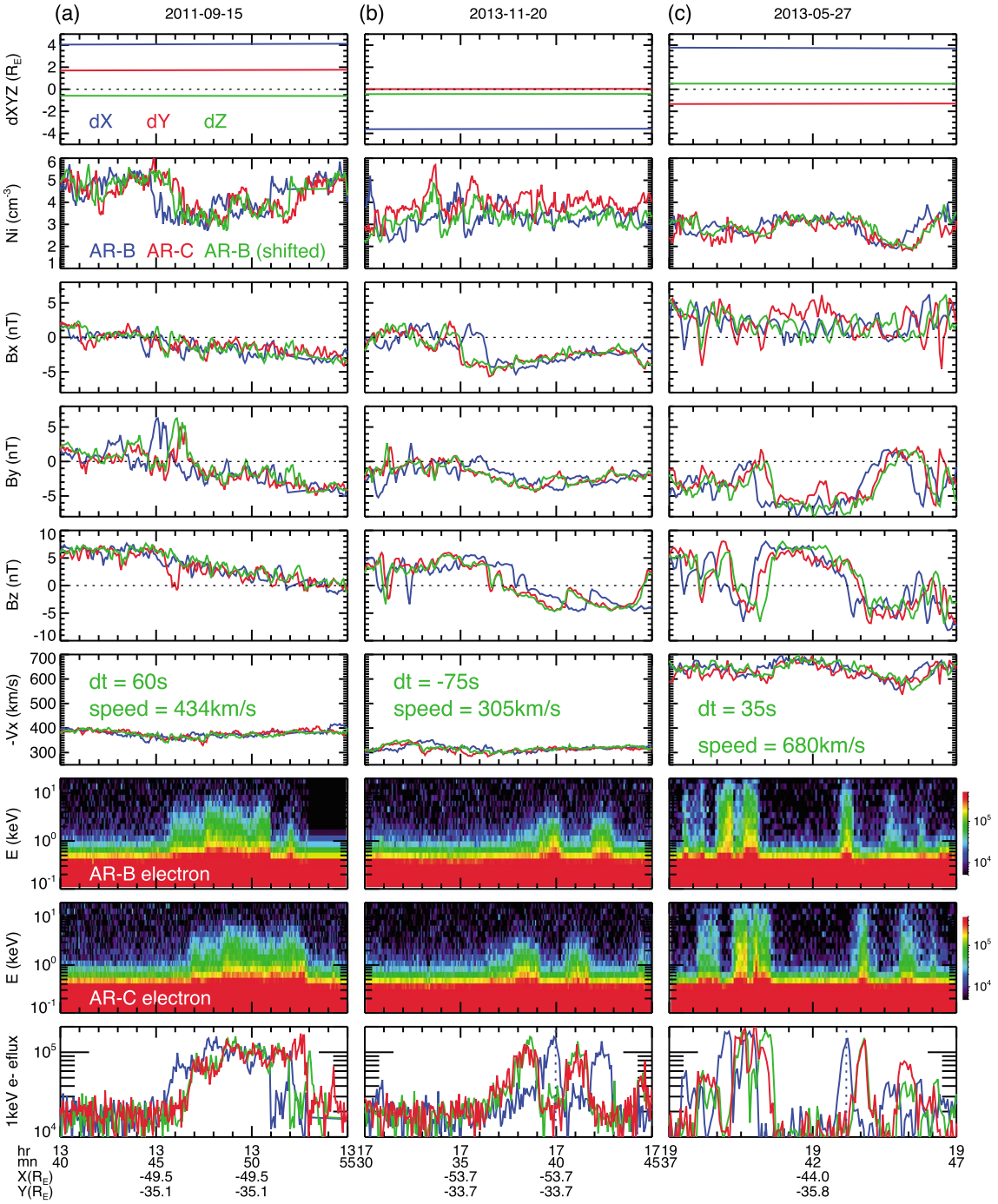

Figure 8. Simultaneous measurements of hot electron enhancements from AR-B and AR-C. (top) Location differences in *X* (blue), *Y* (red), and *Z* (green) (e.g., $dX = X_{\text{AR-B}} - X_{\text{AR-C}}$, AR-B locations are shown in the bottom). (second to bottom) Ion densities, magnetic fields, flow speeds, electron energy flux spectrums, and 1 keV electron energy fluxes observed by AR-B (blue curves) and AR-C (red curves). The green curves are the AR-B profiles shifted with *dt*. The *dt* and propagation speeds are indicated in the $-V_x$ plots.

athickness in the *Z* direction as thin as 1 R_E. Note that since the separation distances and alignments between the two probes keep changing and the hot electron enhancements did not occur all the time, the number of enhancements like those shown in Figures 7 and 8 with specific *X* and *Y* alignments and large separation distances is rather limited in our database. Thus, there are not enough enhancements available so far for statistically determining the spatial scales.

©2014. American Geophysical Union. All Rights Reserved.

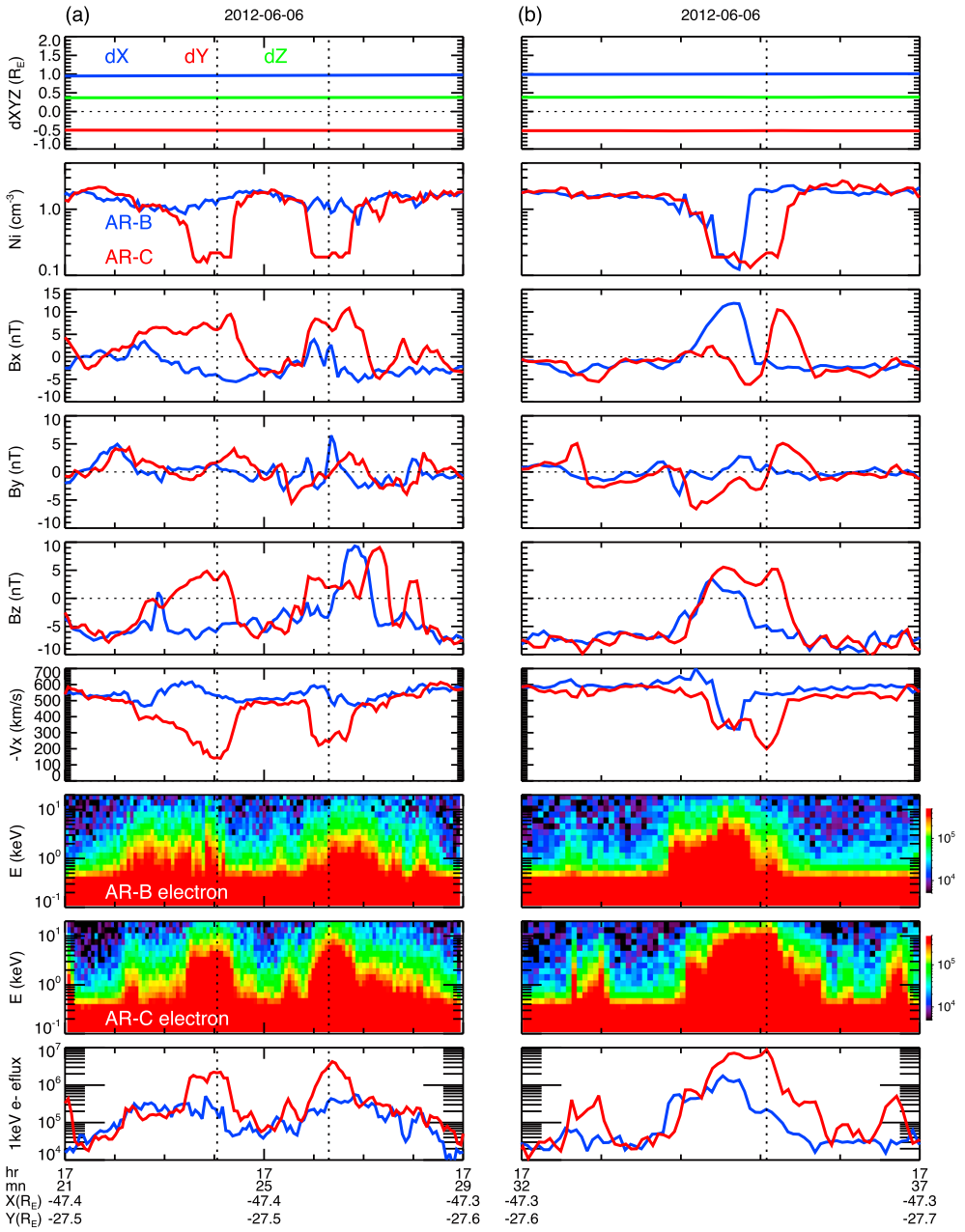

Figure 9. Simultaneous measurements of hot electron enhancements from AR-B and AR-C. (top) Location differences in X (blue), Y (red), and Z (green) (e.g., $dX = X_{AR\text{-}B} - X_{AR\text{-}C}$, AR-B locations are shown in the bottom). (second to bottom) Ion densities, magnetic fields, flow speeds, electron energy flux spectrums, and 1 keV electron energy fluxes observed by AR-B (blue curves) and AR-C (red curves).

4. Discussion

4.1. Processes Generating Hot Electron Enhancements

Many processes have been proposed in the past to explain hot electron enhancements in the magnetosheath, including cold solar wind electrons being energized by bow shock reflection then being advected into the magnetosheath or hot magnetosphere electrons getting access to the magnetosheath either through leakage for a tangential discontinuity magnetopause or through field line merging for a rotational discontinuity magnetopause. For the hot electron enhancements presented in this study, it is difficult for the bow shock process to account for the bursty magnetosphere intrusion observed at the magnetopause and the stronger enhancement seen by the probe closer to the magnetopause.

©2014. American Geophysical Union. All Rights Reserved.

For the hot electrons coming from the magnetosphere, escaping through patchy merging field lines can better explain the bursty and localized enhancements shown in this study than does leakage escape. For example, Figure 4c shows the appearance of cold mantle plasma (~0.5 keV) at ~07:19 UT together with hot magnetosphere electrons in the magnetosphere intrusion, suggesting that the intrusion may be associated with the magnetopause reconnection [e.g., *Hasegawa et al*., 2002; *Wang et al*., 2014]. The observed elongated structure cannot be explained by leakage alone since the gyroradius for 1 keV electrons at 5 nT (5 nT is typical equatorial magnetic field strength in the tail magnetosphere just inside the magnetopause) is only 20 km. But for hot magnetosphere electrons entering the magnetosheath through leakage or reconnection, they can stream away from the magnetopause along the *Y* direction if the magnetosheath magnetic fields have a dominant B_y component. However, as shown in Figure 6, such B_y-dominant magnetic fields are not always seen during the enhancements, suggesting that there may be other responsible processes. Here we propose Kelvin–Helmholtz (K-H) instability as a plausible process.

It has been shown from numerous simulations that the K-H instability occurring at the magnetopause allows cold magnetosheath particles to enter the magnetosphere as well as hot magnetosphere particles to enter the magnetosheath. Subsequent processes at the boundary between the intruding plasma and the surrounding plasma, such as reconnection [e.g., *Nykyri and Otto*, 2001; *Faganello et al*., 2012; *Nakamura et al*., 2013] or diffusion by kinetic Alfvén waves [*Chaston et al*., 2007], would be needed to account for mixing of particles from the magnetosphere and magnetosheath. Therefore, the K-H instability can possibly account for the bursty magnetosphere intrusion into the magnetosheath that results in the larger changes in the magnetosheath properties observed closer to the magnetopause associated with hot electron enhancements, as well as the different mixtures of hot electrons with cold magnetosheath electrons. Note that the reconnection is in principle the same as the previously proposed field line merging process; only here it is secondary to the K-H instability. In the magnetotail, the magnetosheath flow is fast and super magnetosonic. The stability of K-H instability depends on the magnetosoinc speeds on both magnetosphere and magnetosheath sides relative to a perturbation [*Miura and Pritchett*, 1982; *Miura*, 1992]. Simulations by *Kobayashi et al*. [2008] show that a tailward propagating perturbation can be K-H unstable when (1) the flow speeds relative to the perturbation on both sides are slower than the magnetosonic speed or (2) the speed relative to the perturbation in the magnetosheath (magnetosphere) is supermagnetosonic (submagnetosonic). Under the second condition, a shock forms, and the K-H vortex grows downstream of the shock.

Periodic fluctuations of plasma and magnetic fields that are likely due to the K-H instability have been observed by ARTMEIS near the tail magnetopause. As shown in Figure 2, the probes encountered the magnetopause many times from ~4 to 7 UT on 6 June 2012. Several of the encounters are shown in Figure 10a. The probes observed the intrusion of magnetosheath plasma and magnetic field roughly periodically with a period of ~7 min (as indicated by the vertical dotted lines). AR-B is about 1.6 R_E tailward of AR-C and saw the changes in plasma and magnetic fields about 20–25 s later, as illustrated in Figure 5. These suggest that the multiple intrusions are due to wave-like magnetopause perturbations propagating tailward with speed ~490 km/s. The flow speeds on both the magnetosphere and magnetosheath sides relative to this tailward propagating perturbation are found to be submagnetosonic; thus, the K-H instability can possibly be unstable under such flow shear. Figure 10b shows an example around the duskside magnetopause with AR-C in the magnetosheath observing several hot electron enhancements approximately periodically with a period of ~5 min (indicated by the vertical dotted lines). At the same time, AR-B, staying more in the magnetosphere side at similar *X* but was 3 R_E away in *Y* from TH-C, saw repetitively the intrusion of magnetosheath-like cold and dense plasma. The locations for the two probes are illustrated in Figure 5 as if this occurred on the dawnside. The time when AR-C observed one of the hot electron enhancements, AR-B was between two consecutive encounters of magnetosheath intrusion, a connection strongly suggesting that the process responsible for the hot electron enhancements also results in magnetosheath intrusion into the magnetosphere. Note that the wave periods in these two events appear longer than the K-H waves at the near-Earth magnetopause [e.g., *Hasegawa et al*., 2006; *Taylor et al*., 2012], which might be due to vortex merging, compressibility for the strong velocity shear, or some global effects. These two examples suggest the K-H instability and additional subsequent processes at the magnetopause as a plausible process for causing the hot electron enhancements. Therefore, from the point of view of the K-H instability, the magnetosphere intrusion into the magnetosheath and the magnetosheath intrusion into the magnetosphere shown in Figure 5 can be interpreted as resulting from the K-H waves. Along the boundary of intrusion, a current layer may be secondarily produced and reconnection thus induced

©2014. American Geophysical Union. All Rights Reserved.

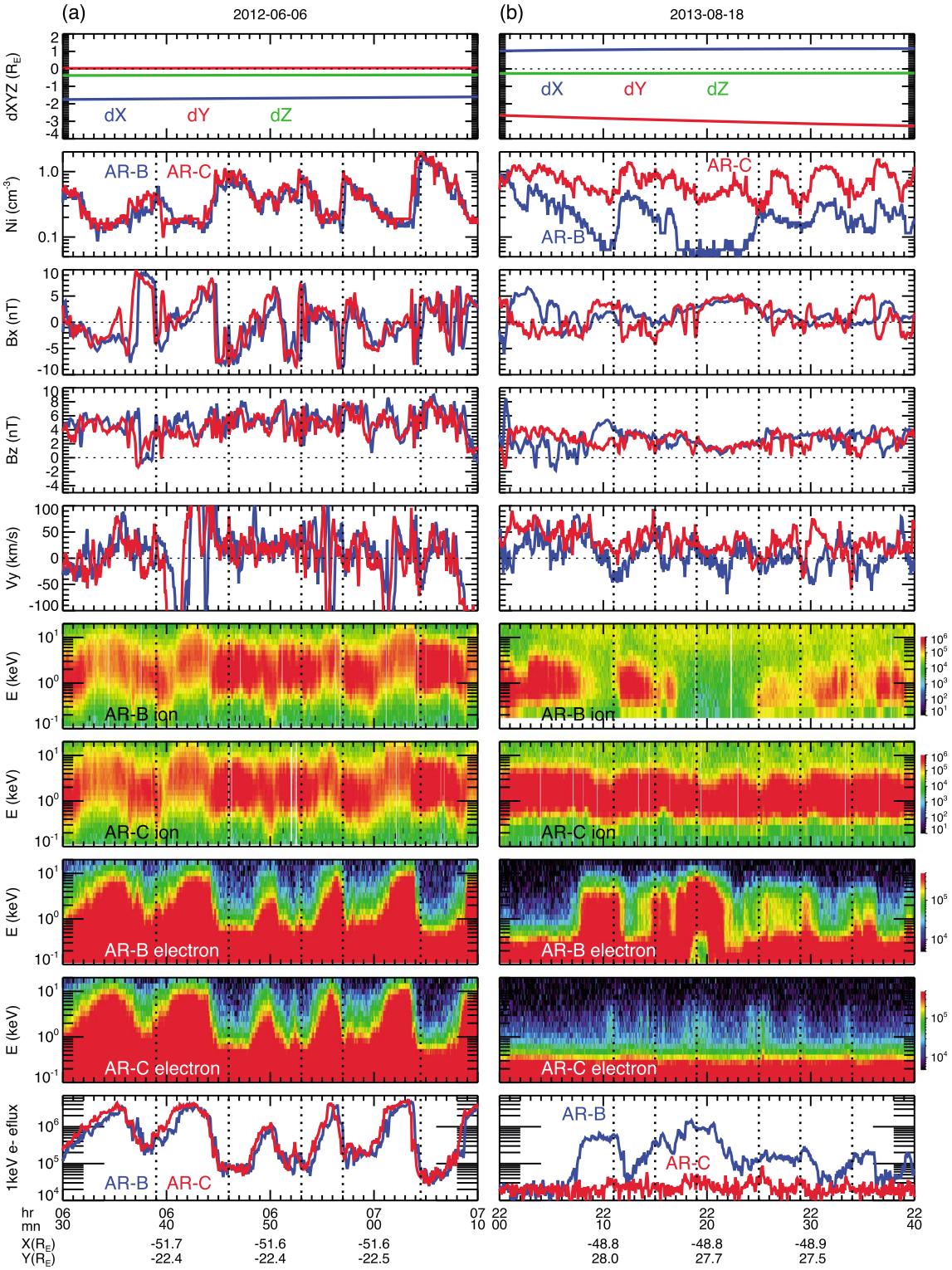

Figure 10. Simultaneous measurements of hot electron enhancements from AR-B and AR-C. (top) Location differences in *X* (blue), *Y* (red), and *Z* (green) (e.g., $dX = X_{AR\text{-}B} - X_{AR\text{-}C}$, AR-B locations are shown in the bottom). (second to bottom) Ion densities, magnetic fields, flow speeds, ion and electron energy flux spectrums, and 1 keV electron energy fluxes observed by AR-B (blue curves) and AR-C (red curves).

©2014. American Geophysical Union. All Rights Reserved.

(maybe in midlatitude region as indicated by 3-D MHD simulations [*Faganello et al*., 2012]), or cross-field diffusion may be induced by kinetic Alfvén waves. The white dotted arrow shown in Figure 5a thus can be interpreted as electrons crossing the boundary through these two secondary processes. To evaluate our suggestion of the K-H instability and subsequent processes as the responsible process requires comparing the observation results presented in this study with K-H simulations. Simulations of the K-H instability with 3-D fully kinetic codes [e.g., *Nakamura et al*., 2013; *Nakamura and Daughton*, 2014], which are capable of modeling electrons of different energies, can provide more appropriate comparison than do simulations with MHD and hybrid codes. Nevertheless, the kinetic simulations have focused on cold magnetosheath ions into the magnetosphere, and there is still difficulty in treating the hot magnetospheric electrons in the 3-D fully kinetic simulations with the present-day supercomputers. Thus, it would not be meaningful to directly compare currently available kinetic K-H simulation results with our observations. Furthermore, the structure of the K-H waves at this ARTEMIS tail region would be largely affected by some global effects like the accelerated shearing flow speed along the magnetopause, the tilted magnetic field at middle-to-high-latitude magnetospheric region that would stabilize the K-H instability or the coupling with the high-latitude (cusp) reconnection. In addition, such global effects may be coupled with the local nonlinear physics of the K-H waves such as secondary tearing instability and secondary Rayleigh–Taylor/K-H instability, which are known to be affected by kinetic effects [e.g., *Nakamura et al*., 2013; *Nakamura and Daughton*, 2014]. To simultaneously consider these global and local physics in numerical simulations and compare the results with the observations shown in this paper, high-resolution global kinetic simulations would be required, which should become feasible in the near future.

The limited number of events presented in this study is not sufficient for determining which of the above processes is dominant, and more studies are needed. Such evaluation can be provided by a statistical study of hot electron enhancements since each of the processes can occur at preferential locations and under preferential conditions of the solar wind, IMF, the magnetosheath, or the magnetosphere. For example, bow shock reflection should create hot electrons predominantly in the duskside magnetosheath [*Sibeck and McEntire*, 1988]. The locations of the magnetopause reconnection in the tail have a dawn-dusk asymmetry depending on the IMF B_y direction [*Sibeck and Lin*, 2014]. The magnetosphere electrons may be hotter on the dawnside due to drift effect, thus may result in stronger enhancements in the dawnside magnetosheath [e.g., *Imada et al*., 2005]. As discussed above, the K-H instability is limited by the magnetosonic speeds in both the magnetosheath and the magnetosphere sides, and the speed conditions are affected by the solar wind, IMF, and geomagnetic activity.

If the magnetospheric electrons are indeed the source for hot electron enhancements as suggested by this study, then it is important to understand the correlation between the magnetospheric conditions and the enhancements. For example, Figures 1 and 2 show that the enhancements occurred at any AE levels, suggesting that the enhancements may not be a direct consequence of substorm activity. In comparison to event 1 shown in Figure 1, hot electron enhancements during event 2 shown in Figure 2 occur more frequently and over a wider magnetosheath Y range, and the peak enhancements are stronger. Figure 7 shows that the keV magnetospheric electron fluxes prior to event 2 are stronger than those prior to event 1. This suggests that the occurrence and strength of enhancements may be a consequence of the magnetospheric conditions. However, the limited number of events of simultaneous two-probe measurements in this study is not sufficient for further investigating such correlations. Furthermore, it remains to be understood on how the tail magnetospheric conditions at $X\sim -60\ R_E$, especially near the magnetopause, are affected by the solar wind, IMF, and magnetosphere activity. Therefore, our next step is to conduct statistical analysis of the dependencies of hot electron enhancements and magnetospheric electrons on locations, the solar wind and IMF conditions, and geomagnetic activity by including more observations from beyond 2013. This will allow for better understanding the correlations between the magnetosphere and the enhancements.

4.2. Pitch Angle Distributions

Pitch angle distributions of the hot electrons in the enhancements may provide indications of the electron origin and underlying processes. However, only a limited number of the enhancements presented in this study have high-time-resolution 3-D phase space density (PSD) distributions available. Figure 11 shows the PSD distributions for the enhancements shown in Figures 6a and 6b. Figure 11a shows that the 1 keV electrons (indicated by the white dotted circles) are quite isotropic in both the magnetosphere intrusions observed by AR-B and the enhancements observed by AR-C.

©2014. American Geophysical Union. All Rights Reserved.

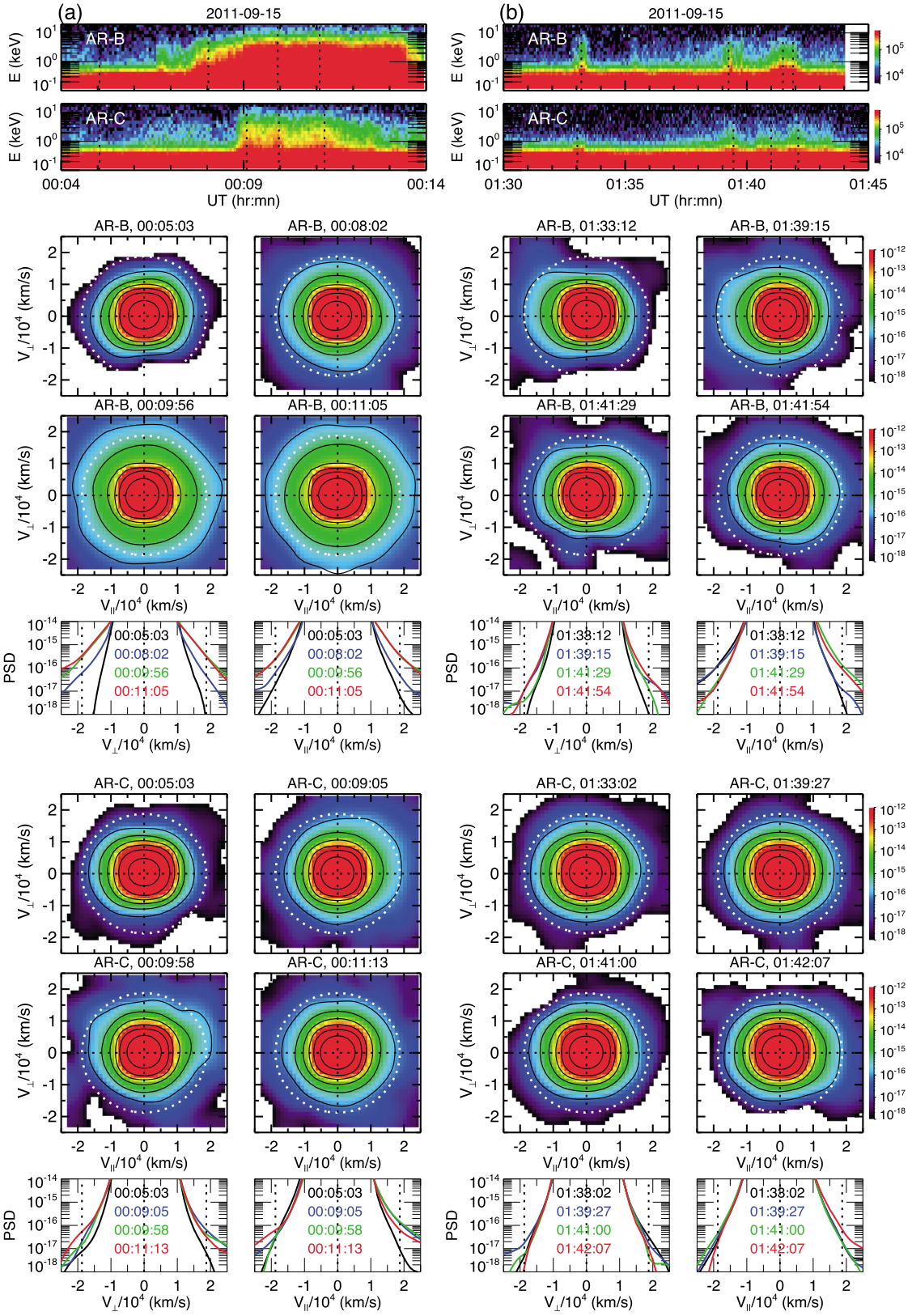

Figure 11. (top to bottom) Electron energy flux spectrums, 2-D electron phase space density ($s^3/km^3/cm^3$) in the $V_\perp$-$V_{||}$ plane and 1-D phase space density as a function of $V_\perp$ or $V_{||}$ at four different times indicated by the vertical dotted lines in the spectrum plot for (a) the events shown in Figure 6a (left column) and (b) the event shown in Figure 6b (right column). The white dotted circles in the 2-D plots indicate the velocity of 1 keV electrons.

©2014. American Geophysical Union. All Rights Reserved.

Sometimes the hot electrons in the enhancements are anisotropic. As shown Figure 11b, AR-B observed distributions to be more field aligned in either the parallel or antiparallel direction. However, such anisotropy is not seen in the same enhancements simultaneously observed by AR-C at the same X and ~4 R_E further outward. More studies are needed in the future to determine whether the anisotropic hot electrons are associated with the processes that create hot electron enhancements, for example, reconnection, and whether there are processes in the magnetosheath that can quickly isotropize these hot electrons, for example, pitch angle scattering by turbulent magnetic fields.

5. Summary

Using simultaneous measurements from the two THEMIS probes with different separation distances and alignments, we have investigated the source, spatial structures, and responsible processes for bursty hot electron enhancements in the tail magnetosheath. The enhancements are typically seen in the 0.5 to 5 keV range with a duration of one to a few minutes. They can be observed at any distance from the magnetopause, but those closer to the magnetopause are more often associated with larger deceases in density and flow speed from the magnetosheath values and with larger changes in magnetic fields.

From simultaneous observations of the two probes on either side of the magnetopause, plasma moments and magnetic fields at the time of the enhancements are found to change to values similar to those of the magnetosphere, suggesting that the changes result from bursty intrusion of the magnetosphere into the magnetosheath and that the hot electrons in these enhancements are magnetosphere electrons. The same enhancement can be simultaneously observed by both probes when they were both in the magnetosheath at the same X but with ~4–7 R_E separation in Y. Also, the probe closer to the magnetopause observes larger changes in the magnetosheath properties with values closer to those of the magnetosphere, indicating that the hot electrons in the enhancements are not locally generated. These observations can be explained by bursty and lateral intrusion of the magnetosphere into the magnetosheath along the Y direction from the magnetopause near the current sheet. The intrusion alters the background magnetosheath plasma and magnetic fields, but the changes become weaker further outward from the magnetopause, causing the smaller changes in the magnetosheath properties observed by the probe farther away from the magnetopause. The hot magnetosphere electrons get access to the magnetosheath following the intrusion and become mixed with the cold magnetosheath electrons. From a limited number of events of simultaneous measurements with different separation distances and alignments, a single-peaked enhancement can have an elongated and thin structure as narrow as 2–3 R_E wide in the X direction, as long as more than 7 R_E in the Y direction, and as thin as 1 R_E in the Z direction.

The hot electron enhancements observed in the tail magnetosheath and the spatial structures presented in this study cannot be satisfactorily explained by hot magnetosphere electrons escaping from merging magnetic field lines and streaming away from the magnetopause along the field lines. The simultaneous observations with periodic hot electron enhancements observed on the magnetosheath side and periodic cold magnetosheath plasma intrusion observed on the magnetosphere side suggest that K-H instability at the magnetopause is a plausibly process for the bursty magnetosphere intrusion and that subsequent reconnection or diffusion can result in the different magnetosphere-magnetosheath particle mixing and magnetosheath property changes observed at different Y distances away from the magnetopause. Comparisons of these observations with the K-H simulations are needed in the future to confirm this suggested role of the K-H instability on the formation of hot electron enhancements.

Acknowledgments

The work by C.-P. Wang and L.R. Lyons has been supported by NASA grant NNX11AJ12G and NSF grant ATM-1003595. The work by X. Xing has been supported by NASA grant NNX12AD11G. We acknowledge NASA contract NAS5-02099 for ARTEMIS, C.W. Carlson and J.P. McFadden for the use of ESA data, and K.H. Glassmeier, U. Auster, and W. Baumjohann for the use of FGM data provided under DLR contract 50 OC 0302. The ARTEMIS data are available online (http://artemis.ssl.berkeley.edu/) for free. We thank J.H. King and N. Papatashvilli at AdnetSystems, NASA GSFC, and CDAWeb for providing the OMNI data.

Yuming Wang thanks the reviewers for their assistance in evaluating this paper.

References

Auster, H. U., et al. (2008), The THEMIS fluxgate magnetometer, *Space Sci. Rev.*, *141*, 235–264, doi:10.1007/s11214-008-9365-9.

Chaston, C. C., M. Wilber, F. S. Mozer, M. Fujimoto, M. L. Goldstein, M. Acuna, M. H. Reme, and A. Fazakerley (2007), Mode Conversion and Anomalous Transport in Kelvin-Helmholtz Vortices and Kinetic Alfven Waves at the Earth's Magnetopause, *Phys. Rev. Lett.*, *99*, 175004, doi:10.1103/PhysRevLett.99.175004.

Faganello, M., F. Califano, F. Pegoraro, T. Andreussi, and S. Benkadda (2012), Magnetic reconnection and Kelvin-Helmholtz instabilities at the Earth's magnetopause, *Plasma Phys. Control. Fusion*, *54*, 124037, doi:10.1088/0741-3335/54/12/124037.

Frank, L. A., J. A. Van Allen, and E. Macagno (1963), Charged-particle observations in the Earth's outer magnetosphere, *J. Geophys. Res.*, *68*(12), 3543–3554, doi:10.1029/JZ068i012p03543.

Hasegawa, H., K. Maezawa, T. Mukai, and Y. Saito (2002), Plasma entry across the distant tail magnetopause 1. Global properties and IMF dependence, *J. Geophys. Res.*, *107*(A5), 1063, doi:10.1029/2001JA900139.

©2014. American Geophysical Union. All Rights Reserved.

Hasegawa, H., M. Fujimoto, K. Takagi, Y. Saito, T. Mukai, and H. Reme (2006), Single-spacecraft detection of rolled-up Kelvin-Helmholtz vortices at the flank magnetopause, *J. Geophys. Res.*, *111*, A09203, doi:10.1029/2006JA011728.

Imada, S., M. Hoshino, and T. Mukai (2005), The dawn-dusk asymmetry in magnetosheath and the leakage of energetic electrons: The Geotail observation, in *Frontiers in Magnetospheric Plasma Physics: Celebrating 10 Years of Geotail Operation*, *Cospar Colloq. Ser.*, vol. 16, edited by M. Hoshino et al., pp. 34–39, Elsevier, New York.

Kobayashi, Y., M. Kato, K. T. A. Nakamura, T. K. M. Nakamura, and M. Fujimoto (2008), The structure of Kelvin–Helmholtz vortices with super-sonic flow, *Adv. Space Res.*, *41*(8), 1325.

Kudela, K., D. G. Sibeck, and M. Slivka (1994), Prognoz 10 energetic particle data: Leakage from the magnetosphere versus bow shock acceleration, *J. Geophys. Res.*, *99*(A12), 23,461–23,472, doi:10.1029/94JA01400.

McFadden, J. P., C. W. Carlson, D. Larson, V. Angelopoulos, M. Ludlam, R. Abiad, B. Elliott, P. Turin, and M. Marckwordt (2008), The THEMIS ESA plasma instrument and in-flight calibration, *Space Sci. Rev.*, *141*, 277–302, doi:10.1007/s11214-008-9440-2.

Meng, C. I., and K. A. Anderson (1970), A layer of energetic electrons (>40 kev) near the magnetopause, *J. Geophys. Res.*, *75*(10), 1827–1836, doi:10.1029/JA075i010p01827.

Miura, A. (1992), Kelvin-Helmholtz instability at the magnetospheric boundary: Dependence on the magnetosheath sonic Mach number, *J. Geophys. Res.*, *97*(A7), 10,655–10,675, doi:10.1029/92JA00791.

Miura, A., and P. L. Pritchett (1982), Nonlocal stability analysis of the MHD Kelvin-Helmholtz instability in a compressible plasma, *J. Geophys. Res.*, *87*(A9), 7431–7444, doi:10.1029/JA087iA09p07431.

Nakamura, T. K. M., and W. Daughton (2014), Turbulent plasma transport across the Earth's low-latitude boundary layer, *Geophys. Res. Lett.*, doi:10.1002/2014GL061952.

Nakamura, T. K. M., W. Daughton, H. Karimabadi, and S. Eriksson (2013), Three-dimensional dynamics of vortex-induced reconnection and comparison with THEMIS observations, *J. Geophys. Res Space Physics*, *118*, 5742–5757, doi:10.1002/jgra.50547.

Nykyri, K., and A. Otto (2001), Plasma transport at the magnetospheric boundary due to reconnection in Kelvin-Helmholtz vortices, *Geophys. Res. Lett.*, *28*(18), 3565–3568, doi:10.1029/2001GL013239.

Sarafopoulos, D. V., M. A. Athanasiu, E. T. Sarris, T. Yamamoto, and S. Kokubun (1999), Properties and origin of energetic particles at the duskside of the Earth's magnetosheath throughout a great storm, *Ann. Geophys.*, *17*, 1121–1133.

Sarafopoulos, D. V., M. A. Athanasiu, D. G. Sibeck, R. W. McEntire, E. T. Sarris, and S. Kokubun (2000), Energetic proton and electron dispersion signatures in the nightside magnetosheath support their leakage out of the magnetopause, *J. Geophys. Res.*, *105*, 15,729–15,740, doi:10.1029/2000JA900041.

Sarris, E. T., S. M. Krimigis, and T. P. Armstrong (1976), Observations of magnetospheric bursts of high-energy protons and electrons at ~ 35 R_E with Imp 7, *J. Geophys. Res.*, *81*(13), 2341–2355, doi:10.1029/JA081i013p02341.

Sarris, E. T., S. M. Krimigis, C. O. Bostrom, and T. P. Armstrong (1978), Simultaneous multispacecraft observations of energetic proton bursts inside and outside the magnetosphere, *J. Geophys. Res.*, *83*(A9), 4289–4305, doi:10.1029/JA083iA09p04289.

Scholer, M., F. M. Ipavich, G. Gloeckler, D. Hovestadt, and B. Klecker (1981), Leakage of magnetospheric ions into the magnetosheath along reconnected field lines at the dayside magnetopause, *J. Geophys. Res.*, *86*(A3), 1299–1304, doi:10.1029/JA086iA03p01299.

Scholer, M., D. Hovestadt, G. Gloeckler, B. Klecker, F. M. Ipavich, and R. D. Zwickl (1984), Magnetospheric ions and electrons in the distant magnetosheath at ~ 50 R_E and ~ 180 R_E: ISEE-3 observations, *Geophys. Res. Lett.*, *11*(10), 1098–1101, doi:10.1029/GL011i010p01098.

Sibeck, D. G., and R. W. McEntire (1988), Multiple satellite observations of leakage of particles from the magnetosphere, *Adv. Space Res.*, *8*(9–10), 201–216.

Sibeck, D. G., and R.-Q. Lin (2014), Size and shape of the distant magnetotail, *J. Geophys Res. Space Physics*, *119*, 1028–1043, doi:10.1002/2013JA019471.

Sibeck, D. G., R. W. McEntire, A. T. Y. Lui, R. E. Lopez, S. M. Krimigis, R. B. Decker, L. J. Zanetti, and T. A. Potemra (1987), Energetic magnetospheric ions at the magnetopause: Leakage or merging?, *J. Geophys. Res.*, *92*(A11), 12,097–12,114, doi:10.1029/JA092iA11p12097.

Sibeck, D. G., et al. (2011), ARTEMIS Science Objectives, *Space Sci. Rev.*, *165*, 59–91, doi:10.1007/s11214-011-9777-9.

Taylor, M. G. G. T., et al. (2012), Spatial distribution of rolled-up Kelvin-Helmholtz vortices at Earth's dayside and flank magnetopause, *Ann. Geophys.*, *30*, 1025–1035, doi:10.5194/angeo-30-1025-2012.

Wang, C.-P., M. Gkioulidou, L. R. Lyons, and V. Angelopoulos (2012), Spatial distributions of the ion to electron temperature ratio in the magnetosheath and plasma sheet, *J. Geophys. Res.*, *117*, A08215, doi:10.1029/2012JA017658.

Wang, C.-P., L. R. Lyons, and V. Angelopoulos (2014), Properties of low-latitude mantle plasma in the Earth's magnetotail: ARTEMIS observations and global MHD predictions, *J. Geophys. Res. Space Physics*, *119*, 7264–7280, doi:10.1002/2014JA020060.

©2014. American Geophysical Union. All Rights Reserved.